COMPARISON OF VORTEX NORMAL MODES IN EASY-PLANE FERROMAGNETS AND ANTIFERROMAGNETS

G. M. Wysin

Department of Physics, Kansas State University, Manhattan, KS 66506 U.S.A.

A. R. Völkel

University of Toronto, Toronto, Ontario, Canada, M5S 1A7
(March 17, 1996)

The spinwave modes associated with magnetic vortices in classical easy-plane ferromagnets (FM) and antiferromagnets (AFM) are studied numerically and compared. We determine the modes about a static vortex through numerical diagonalization on circular systems containing up to several hundred spins on a square lattice, as a function of the anisotropy parameter, $\lambda = J_z/J_{xy}$, where J_z and J_{xy} are the near-neighbor exchange couplings of the indicated spin components. In the FM system, a quasilocal mode is associated with the instability of vortices to transform between in-plane and out-of-plane types at a critical anisotropy $\lambda_c < 1$. In the AFM system, the corresponding instability mode is a true local mode for the out-of-plane vortex. Both systems have degenerate pairs of modes for $\lambda < \lambda_c$, however, these degeneracies split for $\lambda > \lambda_c$ in the FM system but not in the AFM system. We relate this to the presence of a gyrovector for the FM out-of-plane vortex, and corresponding orbital motions associated with the translation modes, both of which are absent for the AFM out-of-plane vortices.

PACS numbers: 75.10.Hk, 75.30.Ds, 75.40.Gb, 75.40.Mg

I. INTRODUCTION

Two-dimensional magnets with easy-plane (xy) symmetry have attracted much attention [1], partly because the unbinding of vortices is responsible for the topological Berezinskii-Kosterlitz-Thouless transition [2,3]. The spin vortices present above the transition temperature T_{KT} are expected to behave like particles and carry effective charges (vorticity or in-plane winding number, and gyrovector or topological charge), and interact with each other via logarithmic pair potentials [4–6]. Assuming they can move about freely in the system, they are also predicted (using an ideal gas theory [7]) to contribute as well to *dynamic* correlation functions, producing the so-called central peak. Just as in one-dimensional soliton-bearing systems, a description of the vortex-spinwave interactions in two-dimensional magnets is necessary for a complete description of the thermodynamics. The spin-wave spectrum in the presence of a vortex or other type of topological excitation also contains information about the stability, internal dynamics, and translational motion of the excitation, considered as a particle-like object. Thus there has been continued interest to understand the interaction of a single vortex with spinwaves [8,9] and even the spinwave fluctuations associated with a vortex-antivortex pair [10]. These studies have used continuum theory, which may not always be a good description of the vortex core, where spatial gradients are large. Our goal here is to present studies using numerical diagonalization on discrete lattice systems to determine the effects

of vortex-spinwave interactions for 2D magnets.

Concerning translational vortex dynamics, an equation due to Thiele [11] for describing the dynamic motion of domain walls was applied by Huber [12] to describe the motion of vortices, under the assumption that a slowly moving vortex does not change its spin structure as a result of the motion. However, moving vortices can do so only by changing their structure, e.g., by excitation of the appropriate translational mode. The excitation of the translational modes is expected to lead to generation of a mass, and modification of the Thiele-Huber equation of motion for vortices [13,14]. Even more alluring is the question of *internal* degrees of freedom. Can there be spinwave modes on a vortex, similar to those found for 1D AFM solitons [15], that correspond to an internal oscillation of the vortex, that may be *localized* on the vortex, and whose frequency is determined only by the exchange constants, not by the system size?

Previous studies of modes of vortices in easy-plane discrete lattice *ferromagnets* [16–18] demonstrated the existence of one particular mode associated with an instability of the vortex at a critical value λ_c of the anisotropy constant $\lambda \equiv J_z/J_{xy} < 1$. The value of λ_c depends on the lattice [19]. For the square lattice, $\lambda_c \approx 0.704$. For $\lambda < \lambda_c$, the stable vortex is *in-plane*, with zero out-of-plane (z) spin components. For $\lambda > \lambda_c$ the stable vortex is *out-of-plane*, with nonzero out-of-plane spin components, whose asymptotic form is known. The mode

responsible for this crossover was found to become soft (small but not zero frequency, due to numerical precision and finite size effects) at $\lambda = \lambda_c$, with a wavefunction having a minimum rms size at this critical point [18]. However, the overall frequency scale of this mode, as well as all other modes in the system, was found to decrease as the inverse system size, which is to say, it is not a *localized* mode. Instead, we can consider it a *quasi-local* mode, especially near λ_c where its rms size is minimum.

The AFM has static in-plane and out-of-plane vortices that are essentially the same as those in the FM, when comparing the spins on a single sublattice. As a result, the AFM exhibits the same in-plane to out-of-plane vortex instability, and the same values for λ_c as in the FM. But for the dynamics, it is a different story. Ivanov *et al.* [20] found the existence of a truly *localized* mode of the out-of-plane AFM vortex. Its rms size and frequency are dependent only on the exchange constants J_z and J_{xy}, provided the system size is large enough compared to the intrinsic rms size. Its existence is linked to the presence of the double continuum spectrum for the AFM; this mode appears in the gap just below the upper continuum. Such localized modes may be observable experimentally through resonance experiments.

The purpose of the present article is to analyze the spinwave spectra in the presence of a vortex for both FM and AFM models, and to present a detailed comparison of their λ-dependence. We will concentrate on the quasi-local and local modes and the translation modes. (The Ivanov *et al.* [20] study concentrated on the properties of the local mode at one value of λ; here we find that this mode is in fact related to the instability mode as $\lambda \to \lambda_c$.) For the translation modes, there is an interesting

distinction between those for the FM and those for the AFM, that is related to the absence or presence, respectively, of symmetry in S^z for the static vortex structure, and also to the corresponding absence or presence of a nonzero gyrovector [16]. This distinction results in orbital motions implied by the FM translation modes, as opposed to linear motions associated with the AFM translation modes. These results are relevant to describing vortex motions via collective coordinate types of theories [14,21,22].

We begin by first reviewing the static vortex structure, then describing the notation for the diagonalization problem, and then relating the notation for the spinwave functions back to the Cartesian spin components and to the continuum limit spherical coordinate angles for the spins. This will be followed by results for FM and AFM models, with a comparison of the similarities and differences.

II. THE STATIC VORTICES

The system to be considered is the classical 2D easy-plane magnet, characterized by near neighbor exchange J and anisotropy parameter λ, with spin Hamiltonian:

$$H = \pm J \sum_{\mathbf{n},\mathbf{a}} (S^x_{\mathbf{n}} S^x_{\mathbf{n+a}} + S^y_{\mathbf{n}} S^y_{\mathbf{n+a}} + \lambda S^z_{\mathbf{n}} S^z_{\mathbf{n+a}}), \quad (2.1)$$

where $(+)$ refers to the AFM and $(-)$ refers to the FM model. The subscript $\mathbf{n}$ labels the lattice site at position $\mathbf{r_n} = (x_{\mathbf{n}}, y_{\mathbf{n}})$, and $\mathbf{a}$ labels the set of displacements to the nearest neighbors. The equations of motion and static vortex solutions as a function of λ for $0 \le \lambda < 1$ are well known [4–6]. Usually it is convenient to represent the spins using "in-plane" (ϕ) and "out-of-plane" (θ) angles,

$$\vec{S}_{\mathbf{n}} = S(\cos\theta_{\mathbf{n}} \cos\phi_{\mathbf{n}}, \cos\theta_{\mathbf{n}} \sin\phi_{\mathbf{n}}, \sin\theta_{\mathbf{n}}). \quad (2.2)$$

For the static vortex at position $\mathbf{r_0} = (x_0, y_0)$, the in-plane angles are given by

$$\phi^0_{\mathbf{n}} = q \tan^{-1}(\frac{y_{\mathbf{n}} - y_0}{x_{\mathbf{n}} - x_0}), \quad (2.3)$$

where the superscripts 0 will be used to indicate quantities associated with static vortex structures. The corresponding out-of-plane component $\sin\theta^0_{\mathbf{n}} = S^z_{\mathbf{n}}/S$ is not described by a simple analytic function, except when $\lambda < \lambda_c$, for which $\theta^0_{\mathbf{n}} = 0$ (See Fig. 1.). For $\lambda > \lambda_c$, the out-of-plane component (on one sublattice for the AFM) has an exponentially decaying asymptotic behavior,

$$S^z_{\mathbf{n}} \approx p\sqrt{\frac{r_v}{r}} e^{-r/r_v}, \quad r_v = \frac{1}{2}\sqrt{\frac{\lambda}{1-\lambda}}, \quad (2.4)$$

where $p = \pm 1$ is the "polarization" of the out-of-plane component, $r = |\mathbf{r_n} - \mathbf{r_0}|$ is the radial distance from the vortex core, and r_v is the vortex core radius. For the FM,
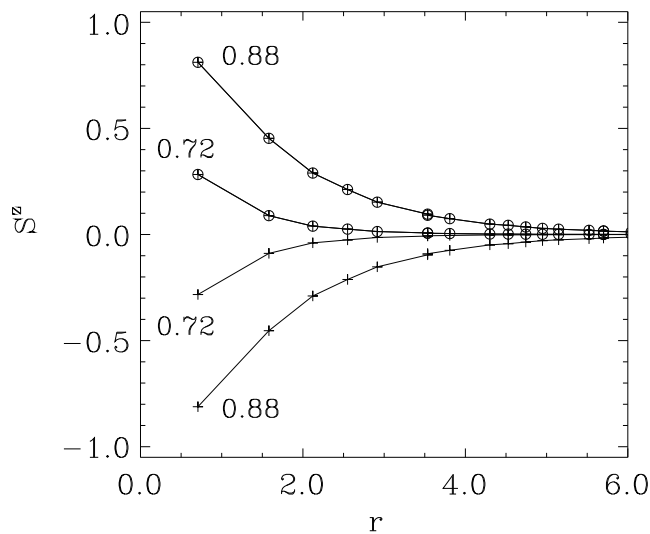

FIG. 1. The out-of-plane spin components in FM (circles) and AFM (+ signs) vortices as a function of radius r from the vortex center, for anisotropy parameters λ as indicated. Both sublattices are shown for the AFM.

the product of vorticity q with polarization p leads to the gyrovector, $\vec{G} = 2\pi pq\hat{e}_z$, which plays an important role in the vortex dynamical equation of motion [12]. ($\vec{G}$ is zero for AFM vortices, due to cancelling contributions from the sublattices.) Elsewhere, for a finite circular system with some radius R, one can use a relaxation procedure [18] for $\lambda > \lambda_c$ to determine the out-of-plane vortex structure. A Dirichlet boundary condition can be applied by extending the lattice to fictitious sites outside the radius R, whose spins are held fixed in the XY-plane along the directions for the static vortex, Eq. 2.3. For a square lattice, some typical out-of-plane vortex structures are shown in Fig. 1. The growth of significant S^z components occurs for AFM and FM models above the same value of $\lambda = \lambda_c$. The structures for a single sublattice of the AFM model are identical to those in the FM model. These are the static vortex structures about which we find the spinwave spectra.

III. THE NORMAL MODE PROBLEM: METHOD

To set up the spinwave calculation about an inhomogeneous state, we use the method in Ref. [18] and define new *local* coordinate axes $\tilde{x}_\mathbf{n}, \tilde{y}_\mathbf{n}, \tilde{z}_\mathbf{n}$, where the $\tilde{z}_\mathbf{n}$ axis is aligned with the unperturbed spin of the static vortex (along $\vec{S}_\mathbf{n}^0$). The $\tilde{x}_\mathbf{n}$ axis is taken in the XY-plane, and then $\tilde{y}_\mathbf{n} = \tilde{z}_\mathbf{n} \times \tilde{x}_\mathbf{n}$. The transformation is

$$
\begin{aligned}
S_\mathbf{n}^x &= -S_\mathbf{n}^{\tilde{x}} \sin\phi_\mathbf{n}^0 - S_\mathbf{n}^{\tilde{y}} \sin\theta_\mathbf{n}^0 \cos\phi_\mathbf{n}^0 + S_\mathbf{n}^{\tilde{z}} \cos\theta_\mathbf{n}^0 \cos\phi_\mathbf{n}^0 \\
S_\mathbf{n}^y &= S_\mathbf{n}^{\tilde{x}} \cos\phi_\mathbf{n}^0 - S_\mathbf{n}^{\tilde{y}} \sin\theta_\mathbf{n}^0 \sin\phi_\mathbf{n}^0 + S_\mathbf{n}^{\tilde{z}} \cos\theta_\mathbf{n}^0 \sin\phi_\mathbf{n}^0 \\
S_\mathbf{n}^z &= S_\mathbf{n}^{\tilde{y}} \cos\theta_\mathbf{n}^0 + S_\mathbf{n}^{\tilde{z}} \sin\theta_\mathbf{n}^0
\end{aligned} \tag{3.1}
$$

Then treating the tilde spin components semiclassically, they are described by an equation of motion, $i\hbar\dot{\vec{S}}_\mathbf{n} = [\vec{S}_\mathbf{n}, H]$. Under linearization in spin components, $\dot{S}_\mathbf{n}^{\tilde{z}} \approx 0$, and a set of equations is obtained for $\dot{S}_\mathbf{n}^{\tilde{x}}$ and $\dot{S}_\mathbf{n}^{\tilde{y}}$ [18].

Solutions for the normal mode problem are sought in the form of creation and annihilation operators $B_k^\dagger$ and B_k, where k is a mode index that includes whatever quantum numbers distinguish the modes, such as principle and azimuthal quantum numbers. These operators are appropriate linear combinations of $S_\mathbf{n}^{\tilde{x}}$ and $S_\mathbf{n}^{\tilde{y}}$:

$$
B_k^\dagger = \sum_\mathbf{n} (w_{k,\mathbf{n}}^{(1)} S_\mathbf{n}^{\tilde{x}} + w_{k,\mathbf{n}}^{(2)} S_\mathbf{n}^{\tilde{y}}) \tag{3.2a}
$$

$$
B_k = \sum_\mathbf{n} (w_{k,\mathbf{n}}^{(1)\,*} S_\mathbf{n}^{\tilde{x}} + w_{k,\mathbf{n}}^{(2)\,*} S_\mathbf{n}^{\tilde{y}}) \tag{3.2b}
$$

with the complex expansion coefficients $w_{k,\mathbf{n}}^{(1)}$ and $w_{k,\mathbf{n}}^{(2)}$ that define the eigenvectors to be determined. Then $B_k^\dagger$ is the creation operator for mode k provided that the coefficients $w_{k,\mathbf{n}}^{(1,2)}$ are chosen so that $\dot{B}_k^\dagger = i\omega_k B_k^\dagger$, where ω_k is the normal mode (spinwave) frequency, also to be

determined. The corresponding matrix for this diagonalization problem has elements that depend on the static structure, $\theta_\mathbf{n}^0, \phi_\mathbf{n}^0$. Once the eigenvectors are known, the spin components are recovered through the inverse relationship to Eq. (3.2), specifically,

$$
S_\mathbf{n}^{\tilde{x}} = iS \sum_k (w_{k,\mathbf{n}}^{(2)} B_k - w_{k,\mathbf{n}}^{(2)\,*} B_k^\dagger) \tag{3.3a}
$$

$$
S_\mathbf{n}^{\tilde{y}} = -iS \sum_k (w_{k,\mathbf{n}}^{(1)} B_k - w_{k,\mathbf{n}}^{(1)\,*} B_k^\dagger) \tag{3.3b}
$$

For the creation and annihilation operators to satisfy the standard commutation relation, $[B_k, B_{k'}^\dagger] = \delta_{k,k'}$, the eigenvectors must be normalized by the requirement,

$$
\hbar S \sum_\mathbf{n} [(iw_{k,\mathbf{n}}^{(1)\,*} w_{k,\mathbf{n}}^{(2)}) + (iw_{k,\mathbf{n}}^{(1)\,*} w_{k,\mathbf{n}}^{(2)})^*] = 1. \tag{3.4}
$$

This requirement is necessary primarily if one is interested in a thermal population of the modes, and wants to know the absolute magnitudes of the thermal fluctuations associated with the modes.

For our discussion here, we are instead more interested in the time dependent spin motions associated with each mode, in order to understand the role of the mode in the vortex instability, translation or internal oscillation. In this case the absolute normalization is not so important, however, the relation of the eigenvector coefficients $w_{k,\mathbf{n}}^{(1,2)}$ to the angular coordinates is useful. If we suppose that one mode k is excited from the "ground state", which is the static vortex, then the mixture of the excited state with the ground state leads to the time dependent local spin fluctuations,

$$
\langle S_\mathbf{n}^{\tilde{x}}(t) \rangle = \mathrm{Re}\{-w_{k,\mathbf{n}}^{(2)\,*} e^{i\omega_k t}\}, \quad \langle S_\mathbf{n}^{\tilde{y}}(t) \rangle = \mathrm{Re}\{w_{k,\mathbf{n}}^{(1)\,*} e^{i\omega_k t}\}. \tag{3.5}
$$

Essentially, $w_{k,\mathbf{n}}^{(2)}$ relates to fluctuations of spin components that are only within the original xy-plane, while $w_{k,\mathbf{n}}^{(1)}$ contains spin fluctuations that are a combination of in-plane and out-of-plane spin components. In the case where the static spin is in the xy-plane, $w_{k,\mathbf{n}}^{(1)}$ involves only out-of-plane fluctuations. This can be seen more readily by relating these coordinates to the more usual angular coordinates. If we consider the perturbation of site $\mathbf{n}$ in the form, $\phi_\mathbf{n} = \phi_\mathbf{n}^0 + \varphi_\mathbf{n}$, and $\theta_\mathbf{n} = \theta_\mathbf{n}^0 + \vartheta_\mathbf{n}$, with $\varphi_\mathbf{n}, \vartheta_\mathbf{n} \ll 1$, then substitution into Eqs. (2.2) and (3.1) leads to the result,

$$
S_\mathbf{n}^{\tilde{x}} = S\varphi_\mathbf{n} \cos\theta_\mathbf{n}^0, \quad S_\mathbf{n}^{\tilde{y}} = S\vartheta_\mathbf{n}. \tag{3.6}
$$

This confirms that $S_\mathbf{n}^{\tilde{x}}$ or $w_{k,\mathbf{n}}^{(2)}$ relate purely to in-plane oscillation $\varphi_\mathbf{n}$, and $S_\mathbf{n}^{\tilde{y}}$ or $w_{k,\mathbf{n}}^{(1)}$ relate to oscillations that change the amount of out-of-plane tilting of $\vec{S}_\mathbf{n}$ (although this latter motion can contain fluctuations of both in-plane and out-of-plane spin components).

IV. RELATION OF WAVEFUNCTIONS TO CONTINUUM LIMIT ANGLES

In the FM model, the angles $\vartheta_{\mathbf{n}}$ and $\varphi_{\mathbf{n}}$ that are given by the coefficients $w_{k,\mathbf{n}}^{(1)}$ and $w_{k,\mathbf{n}}^{(2)}$, respectively, can be replaced by their continuum counterparts, $\vartheta(\vec{r})$ and $\varphi(\vec{r})$. For the AFM model, however, the presence of multiple sublattices means that appropriate linear combinations of the $w^{(1,2)}$ coefficients on different sublattices will map over into slowly varying continuum angles to describe the spin field. The simplest case is that of bipartite lattices such as square and honeycomb. If $\mathbf{n}$ is a site of one sublattice, and $\mathbf{n}+\mathbf{a}$ is a neighboring site on the other sublattice, then it is usual to define a dimensionless continuum magnetization vector $\vec{m}(\mathbf{r})$ and sublattice magnetization vector $\vec{\ell}(\mathbf{r})$ as [15]

$$\vec{m} = (\vec{S}_{\mathbf{n}} + \vec{S}_{\mathbf{n}+\mathbf{a}})/2S, \qquad (4.1a)$$

$$\vec{\ell} = (\vec{S}_{\mathbf{n}} - \vec{S}_{\mathbf{n}+\mathbf{a}})/2S, \qquad (4.1b)$$

for position $\mathbf{r} = \mathbf{n} + \mathbf{a}/2$. In the case of small deviations from the antiferromagnetic state, which corresponds to small gradients on an individual sublattice, and slow time dependence or low frequency motion, we have $|\vec{\ell}| \approx 1$, and $|\vec{m}| \ll 1$. More precisely, the conserved individual spin length, $|\vec{S}_{\mathbf{n}}| = S$ leads to the conditions, $\vec{m} \cdot \vec{\ell} = 0$, $\vec{m}^2 + \vec{\ell}^{\,2} = 1$.

Definitions (4.1) can lead to a nonzero $\vec{m}$ in the vicinity of the core of a static AFM vortex, which is an unphysical result, because static solutions in the presence of strong AFM exchange should result in $\vec{m} = 0$. Alternatively, a more controlled way to define ferromagnetic and antiferromagnetic vectors is to define two continuum spin fields $\vec{S}_A(\mathbf{r})$ and $\vec{S}_B(\mathbf{r})$, in terms of *continuous* $\vec{\ell}(\mathbf{r})$ and $\vec{m}(\mathbf{r})$ vectors via

$$\vec{S}_A(\mathbf{r}) = S[\vec{m}(\mathbf{r}) + \vec{\ell}(\mathbf{r})], \quad \vec{S}_B(\mathbf{r}) = S[\vec{m}(\mathbf{r}) - \vec{\ell}(\mathbf{r})],$$
$$(4.2)$$

We again see that with the requirement, $|\vec{S}_A| = |\vec{S}_B| = S$, the conditions, $\vec{m}(\mathbf{r}) \cdot \vec{\ell}(\mathbf{r}) = 0$, $\vec{m}(\mathbf{r})^2 + \vec{\ell}(\mathbf{r})^2 = 1$, must hold. These fields are assumed to have small gradients and are assumed to be defined at any positions in the plane. $\vec{S}_A(\mathbf{r})$ maps onto the spins of one sublattice (say, the sites $\mathbf{n}$) and $\vec{S}_B(\mathbf{r})$ maps onto the sites of the other sublattice (the sites $\mathbf{n} + \mathbf{a}$). As above, taking $\mathbf{r}$ to be between the sites $\mathbf{n}$ and $\mathbf{n} + \mathbf{a}$; $\mathbf{r} = \mathbf{n} + \mathbf{a}/2$,

$$\vec{S}_{\mathbf{n}} = \vec{S}_A(\mathbf{r} - \mathbf{a}/2) = S[\vec{m}(\mathbf{r} - \mathbf{a}/2) + \vec{\ell}(\mathbf{r} - \mathbf{a}/2)], \quad (4.3a)$$

$$\vec{S}_{\mathbf{n}+\mathbf{a}} = \vec{S}_B(\mathbf{r} + \mathbf{a}/2) = S[\vec{m}(\mathbf{r} + \mathbf{a}/2) - \vec{\ell}(\mathbf{r} + \mathbf{a}/2)].$$
$$(4.3b)$$

Expanding these in Taylor series about the point $\mathbf{r}$, and supposing that $|\vec{\ell}| \approx 1$, while $|\vec{m}| \ll 1$, with the gradient operation also a "small quantity" ($\nabla \vec{\ell}$ similar in magnitude to $\vec{m}$), leads to approximate expressions

$$\vec{m}(\mathbf{r}) = (\vec{S}_{\mathbf{n}} + \vec{S}_{\mathbf{n}+\mathbf{a}})/2S + (\frac{\mathbf{a}}{2} \cdot \nabla)\vec{\ell}(\mathbf{r}), \qquad (4.4a)$$

$$\vec{\ell}(\mathbf{r}) = (\vec{S}_{\mathbf{n}} - \vec{S}_{\mathbf{n}+\mathbf{a}})/2S, \qquad (4.4b)$$

where second and higher order quantities have been dropped. The first equation shows that it is possible to have $\vec{m}(\mathbf{r}) = 0$ and $(\vec{S}_{\mathbf{n}} + \vec{S}_{\mathbf{n}+\mathbf{a}}) \neq 0$ when a gradient of $\vec{\ell}$ is present, such as in the vicinity of a vortex core. In the presence of local AFM order, $\vec{m}(\mathbf{r}) = 0$, however, it is possible to have a nonzero gradient of the AFM order, $\mathbf{a} \cdot \nabla \vec{\ell}$. Furthermore, since $|\vec{\ell}| \approx 1$, *both* terms in Eq. (4.4a) are of the same order ($\mathbf{a} \cdot \nabla$), and must be included in the expansion [23]. For these reasons, the equations (4.4) are preferred over the less precise equations (4.1).

We would like to relate spherical coordinate angles for $\vec{\ell}(\mathbf{r})$ to appropriate combinations of the $w^{(1,2)}$ coefficients. Thus, define the angles for $\vec{\ell}(\mathbf{r})$ using

$$\vec{\ell} = (\cos\theta_\ell \cos\phi_\ell, \cos\theta_\ell \sin\phi_\ell, \sin\theta_\ell). \qquad (4.5)$$

The static vortex structure will possess a finite $\vec{\ell}$, with angles $\theta_\ell^0, \phi_\ell^0$, and $\vec{m} = 0$. Static $\vec{m}$ will be produced in this model only if an applied magnetic field is present. The static structure of $\vec{\ell}$ in an AFM vortex is the same as the static structure of $\vec{S}$ in an FM vortex, and has a small spatial gradient, especially near the vortex core. The gradient cancels the first term in Eq. (4.4a), and $\vec{m} = 0$ results. The dynamic perturbation of this structure leads to deviations: $\theta_\ell = \theta_\ell^0 + \vartheta_\ell$, $\phi_\ell = \phi_\ell^0 + \varphi_\ell$. These deviations ϑ_ℓ and φ_ℓ relate to the normal mode wavefunction coefficients $w^{(1)}$ and $w^{(2)}$ respectively, through Eqs. (4.4b), (3.5) and one like (3.6) for $\vec{\ell}$.

Under the assumption of small gradients, and $\vec{S}_{\mathbf{n}}^0 \approx -\vec{S}_{\mathbf{n}+\mathbf{a}}^0$ for the static structure, we will have approximate relations between the local coordinate axes on neighboring sites, one on each sublattice:

$$\tilde{x}_{\mathbf{n}+\mathbf{a}} \approx -\tilde{x}_{\mathbf{n}}, \quad \tilde{y}_{\mathbf{n}+\mathbf{a}} \approx \tilde{y}_{\mathbf{n}}, \quad \tilde{z}_{\mathbf{n}+\mathbf{a}} \approx -\tilde{z}_{\mathbf{n}}, \qquad (4.6)$$

This will not be valid close to the vortex core where $\nabla\vec{\ell}$ is large, however, elsewhere it is a good approximation. Using it in Eq. (4.4b), leads to an expression,

$$\vec{\ell} \approx \tilde{z}_{\mathbf{n}} + \left(\frac{\vec{S}_{\mathbf{n}}^{\tilde{x}} + \vec{S}_{\mathbf{n}+\mathbf{a}}^{\tilde{x}}}{2S}\right)\tilde{x}_{\mathbf{n}} + \left(\frac{\vec{S}_{\mathbf{n}}^{\tilde{y}} - \vec{S}_{\mathbf{n}+\mathbf{a}}^{\tilde{y}}}{2S}\right)\tilde{y}_{\mathbf{n}}. \quad (4.7)$$

On the other hand, an equation like (3.6) also holds for $\vec{\ell}$, namely,

$$\vec{\ell} \approx \tilde{z}_{\mathbf{n}} + \varphi_\ell \cos\theta_\ell^0 \ \tilde{x}_{\mathbf{n}} + \vartheta_\ell \ \tilde{y}_{\mathbf{n}}. \qquad (4.8)$$

4

Then the direct comparison of these results together with Eq. (3.5) shows that the dynamic parts of $\vec{\ell}$ are [20]

$$\ell^{\tilde{x}} = \varphi_\ell \cos\theta_\ell^0 = \mathrm{Re}\{-\frac{w_{k,\mathbf{n}}^{(2)\,*} + w_{k,\mathbf{n+a}}^{(2)\,*}}{2S}e^{i\omega_k t}\}, \quad (4.9a)$$

$$\ell^{\tilde{y}} = \vartheta_\ell = \mathrm{Re}\{\frac{w_{k,\mathbf{n}}^{(1)\,*} - w_{k,\mathbf{n+a}}^{(1)\,*}}{2S}e^{i\omega_k t}\}. \quad (4.9b)$$

Eq. (4.9a) contains purely in-plane movements of $\vec{\ell}$, while Eq. (4.9b) corresponds to time-dependent out-of-plane tilting of $\vec{\ell}$. It is assumed here that only one particular mode k is excited on the vortex.

The above results show that it is possible to determine the continuum angles for $\vec{\ell}$ in terms of the wavefunction coefficients; it is clear this can be extended to find the corresponding mapping for continuum angles associated with $\vec{m}$. For our results from discrete lattice diagonalizations, we will generally present pictures of the wavefunction complex coefficients only, represented as arrows in the plane, from which $\vec{\ell}$ and $\vec{m}$ can be determined. The advantage of this will become clear; particular modes in the AFM can appear to have either acoustic or optical nature, depending on whether the two sublattices move in-phase or out-of-phase, respectively. We will also see that this aspect is closely coupled to whether the mode has weak or strong out-of-plane motions, respectively.

V. SOME DETAILS OF THE DIAGONALIZATIONS

The systems used for either ferro- or antiferromagnetic exchange were setup as follows. A circular section of desired radius R was cut out of a larger square lattice of sites, with the center of the circle coincident with the center of a unit cell. The spins on sites within the circular system and also outside it were then set to point in the directions of a static in-plane vortex, Eq.(2.3), however, the four sites nearest to the vortex center were given small S^z components. Then the sites within the circle were allowed to relax according to the procedure in [18], to the appropriate vortex structure for the given value of λ (in-plane or out-of-plane vortex). During the relaxation procedure, the sites outside of the circle were held fixed in their in-plane vortex directions. This then sets a kind of Dirichlet-vortex boundary condition.

The normal mode problem and matrix was setup by considering the perturbation around this initial configuration inside the circular system, but where its boundary sites interact also with sites outside of the circle, still held in the directions for the static in-plane vortex. Further details of the definition of the normal mode matrix are found in Reference [18].

Diagonalizations were performed on a Sun Sparc-20 with 128MB RAM, for FM and AFM models using a range of λ between 0 and 1, and system radii R from 5 to 21. The system with $R = 21$ contains 1396 sites, and is the largest system that we could do by this method, requiring the storage of $(2 \times 1396)^2$ matrix elements (2 degrees of freedom per site), and an equal number of elements of the eigenvectors. Although the matrix is sparse, it is not symmetric nor even Hermitian, so the EISPACK subroutine, RG (real general matrix) was used to find the eigenspectrum, in double precision. The complete eigenspectrum (eigenvalues and wavefunctions) was saved for two closely spaced values of λ, to allow for tracking of the modes with changing λ, and this also increased the memory requirements (possible only for $R \le 19$).
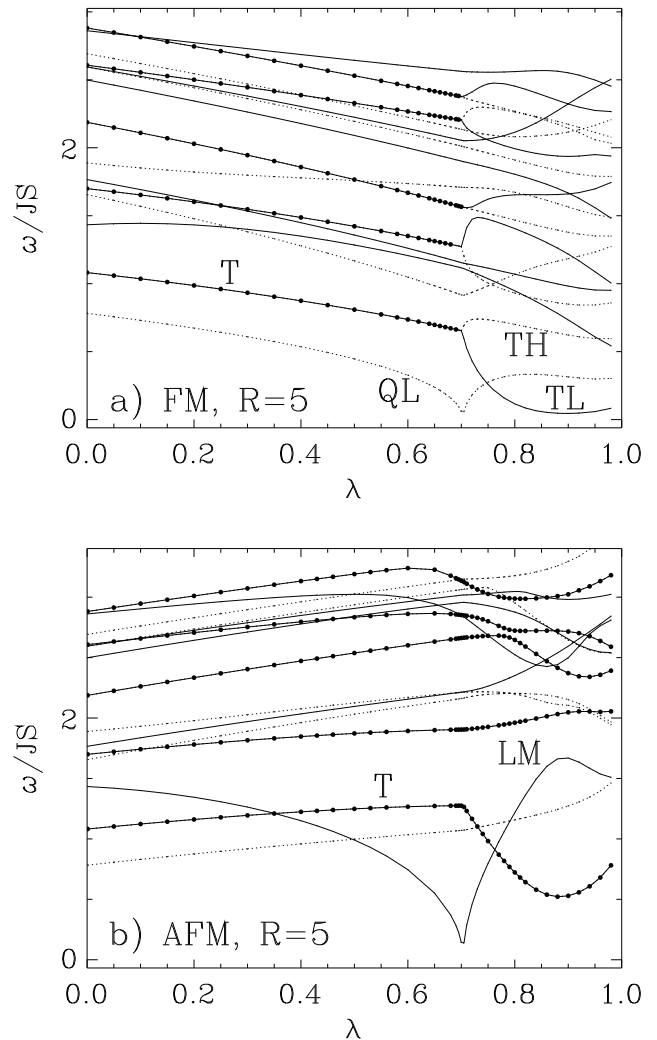

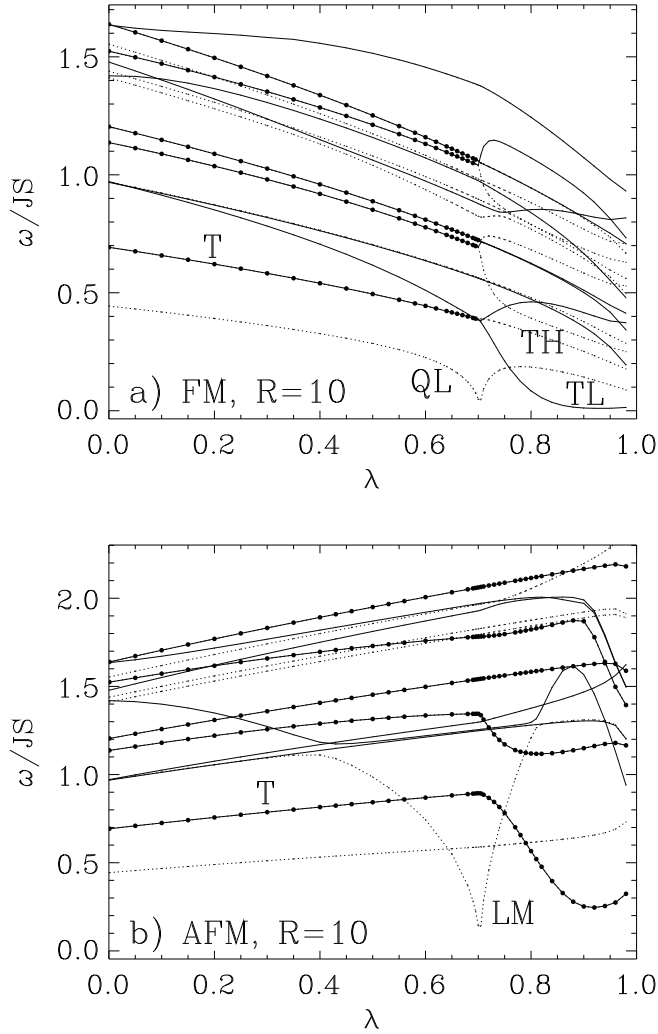
FIG. 2. The lowest frequency modes as a function of anisotropy parameter λ, for a radius $R = 5$ system, containing 80 sites: a) FM, b) AFM. Here and in Figs. 3 and 4 doubly degenerate modes are indicated by the solid data points. Solid and dotted lines are used only to distinguish nearby modes. T, TL, and TH refer to the translation modes, and QL and LM denote the quasi-local and local modes for the FM and AFM systems, respectively.

VI. RESULTS: COMPARISONS OF RESULTS
FOR FM AND AFM

Next we show some typical results for the FM and AFM models, where the only difference between the two models is the sign of the exchange constant.

A. Spectra

Some eigenfrequency spectra of the lowest modes versus λ for both models are shown in Figs. 2, 3 and 4, for systems with radii $R = 5, R = 10$, and $R = 15$, respectively. In these Figures, the different line styles are used to distinguish nearby modes, and solid circles are used to indicate doubly degenerate modes.

Both the FM and AFM models exhibit the crossover from in-plane to out-of-plane static vortex, as seen by the presence of interesting features around $\lambda_c \approx 0.70$. These features include downward cusps in some modes at λ_c, breaking of degeneracies in the FM mode at λ_c, and more subtle changes in some of the modes (such as downward turns) for the AFM model at λ_c.

In the FM, modes that are degenerate below λ_c split suddenly at λ_c into higher and lower components. In Ref. [18], the splitting was found to be associated with a "winding number" or azimuthal quantum number m for the mode, which determines how the phase of its wavefunction changes with azimuthal coordinate. We have the following approximate continuum description of the wavefunctions far from the vortex core:

$$w_k^{(1,2)}(r, \chi) \propto f_k^{(1,2)}(r)e^{im\chi}, \qquad (6.1)$$

FIG. 3. The lowest frequency modes as a function of anisotropy parameter λ, for a radius $R = 10$ system, containing 316 sites: a) FM, b) AFM.
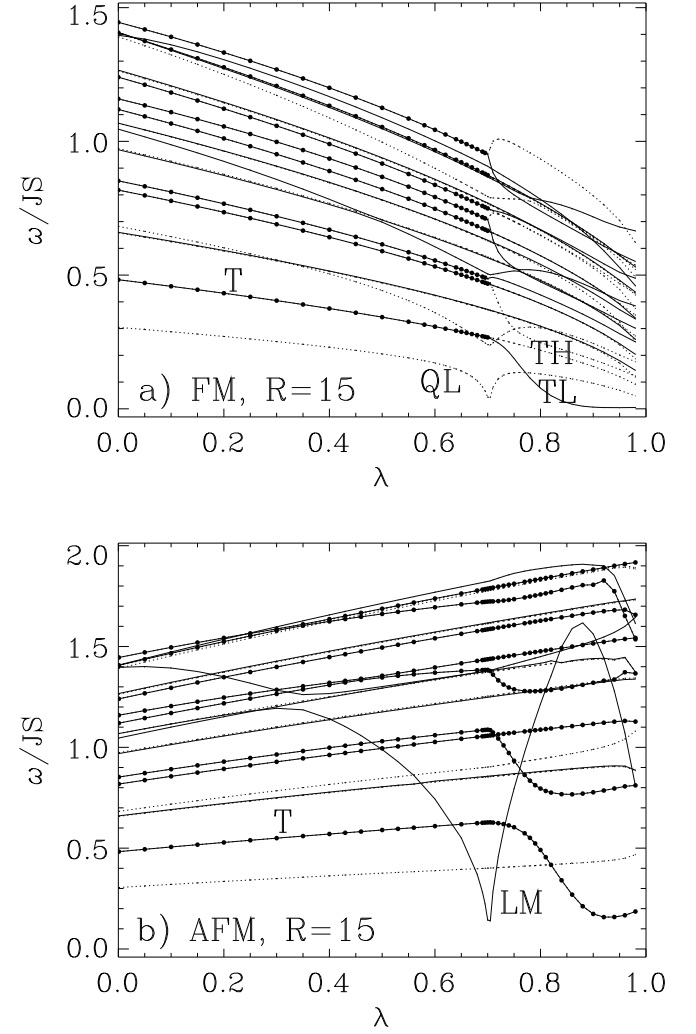
FIG. 4. The lowest frequency modes as a function of anisotropy parameter λ, for a radius $R = 15$ system, containing 716 sites: a) FM, b) AFM.

where the winding number m is an integer, (r, χ) are the polar coordinates of a position in the system, and $f_k^{(1,2)}(r)$ determines the radial dependence. For $\lambda < \lambda_c$, the in-plane vortex has modes with $\pm m$ that are degenerate. For $\lambda > \lambda_c$, the presence of static S^z components for the out-of-plane vortex causes the $+m$ and $-m$ modes to become nondegenerate — the out-of-plane polarization $p = \pm 1$ of the vortex induces a preferred sense of phase change of the spinwave mode that has lower frequency. In general, for vorticity $q = +1$, polarization $p = +1$, the mode with $m < 0$ falls below the mode with with $m > 0$. (Also see Section VI C below for wavefunction diagrams.) In fact, it is possible to show [24] that the continuum equation of motion for the perturbation $\dot{\vartheta}$ contains one term proportional to

$$S_z^0 \nabla \phi^0 \cdot \nabla \vartheta \propto pqm \propto Gm, \qquad (6.2)$$

and similarly for φ, where $G = 2\pi pq$ is the z-component of the gyrovector. Therefore, for $m \neq 0$ modes, if the gyrovector is present, a splitting will occur.

The most obvious difference of the AFM spectra compared to the FM spectra is the persistence of the degeneracies for $\lambda > \lambda_c$. This is due to the symmetry of the AFM out-of-plane vortex with respect to reversing its static S^z spin components and simultaneously interchanging the sublattices. To the contrary, the static FM out-of-plane vortex does not possess this symmetry. Below we discuss this more fully with respect to the translation modes, which have winding numbers $m = \pm 1$ and are degenerate below λ_c, and remain degenerate above λ_c for the AFM model, but split for the FM model, as discussed above. This difference is interesting because it accounts for the particularly different motional properties of the out-of-plane vortices of the two models, an aspect that has been previously linked to the presence (FM) or absence (AFM) of the vortex gyrovector [16,25].

Finally, the other important difference between the FM and AFM models can be seen by comparing the spectra for different sized systems. For the FM model, increasing the system size results in lowering the frequencies of all of the modes; the frequencies diminish approximately as $1/R$ at fixed λ. For the AFM model, this result also holds for most of the modes, except that there is one mode in particular whose frequency is approximately unaffected by system size, although it is seen to mix with nearby modes. This interesting mode has its frequency determined primarily by λ, rather than R, indicating that it is truly intrinsic to the vortex, and not a result of boundary conditions. For $\lambda > \lambda_c$, it is the localized mode discussed by Ivanov *et al.* [20].

B. The Instability Mode and Local Mode

For $\lambda < \lambda_c$, the in-plane vortex in each model has the "instability mode" with a downward cusp approaching close to zero frequency as $\lambda \to \lambda_c$. For the FM model,

this is the lowest frequency mode for any $\lambda < \lambda_c$, whereas for the AFM model, the instability mode is the lowest frequency mode only for λ near λ_c. For the FM model, even the frequency of the instability mode diminishes with increasing system size as approximately $1/R$. Because the wavefunction associated with this mode has an rms radius that approaches zero near λ_c, it can be considered a "quasi-local" mode for the FM vortices. (Marked by QL in the Figures.)

For the AFM, however, this instability mode is identified with the truly localized mode mentioned above. (Marked by LM in the Figures.) It is seen that it mixes with other modes, depending on the system size, but far from the values of λ where the mixing occurs, its wavefunction has a simple form expected for this instability mode, with winding number $m = 0$. On the other hand, as λ approaches zero (XY-limit), the instability mode in the AFM model can go through a set of different mixings with other modes (the number depends on the system size; there is no mixing for the $R = 5$ system), until approaching a frequency around 1.4 for $\lambda = 0$. The limiting value of $\omega = 1.4$ does *not* depend on the system size. For the out-of-plane vortex spectrum, this same mode reaches a maximum frequency of about $\omega = 1.6$ for $\lambda \approx 0.88$, and these numbers also do not depend on the system size. These results hold because this mode is the same as the local mode found in Ref. [20], whose properties are only determined by λ, provided that the system size is larger than the vortex core length scale r_v [Eq. (2.4)]. However, that work considered only the case of λ approaching 1 (Heisenberg limit), where the continuum theory is a valid description of the spin dynamics on the discrete lattice. Thus, it is especially interesting to see this lack of system size dependence for this mode even for λ approaching zero.

1. FM: Instability Mode Wavefunction

The wavefunction for any mode is easily represented by using arrows in the plane for each of the complex amplitudes, $w_{k,\mathbf{n}}^{(1)}$ and $w_{k,\mathbf{n}}^{(2)}$, where the angle of the arrow measured from the x-axis is the phase of the complex amplitude. These kinds of diagrams were used in Ref. [18] and [20]. Such diagrams for the FM instability mode are shown in Fig. 5, for the $R = 10$ system, at different values of λ. We use open arrows ($\longrightarrow$) to represent $w_{k,\mathbf{n}}^{(1)}$ (out-of-plane fluctuations) and closed arrows ($\longrightarrow\!\!\!\triangleright$) to represent $w_{k,\mathbf{n}}^{(2)}$ (in-plane fluctuations). It was necessary in these diagrams either to exaggerate the $w_{k,\mathbf{n}}^{(1)}$ or $w_{k,\mathbf{n}}^{(2)}$ arrows such that both could be seen on the same diagram.

For the FM instability mode, there is a considerable concentration of the amplitude $w_{k,\mathbf{n}}^{(1)}$ around the vortex core for λ approaching close to λ_c, and the phase of the wavefunction is constant around the vortex. This means that the winding number is $m = 0$. Further analysis of

a) QL, λ=0.0, ω/JS=0.4437

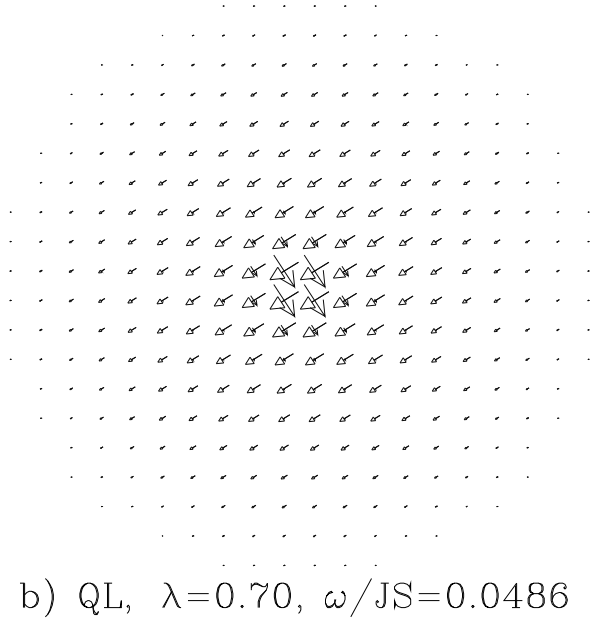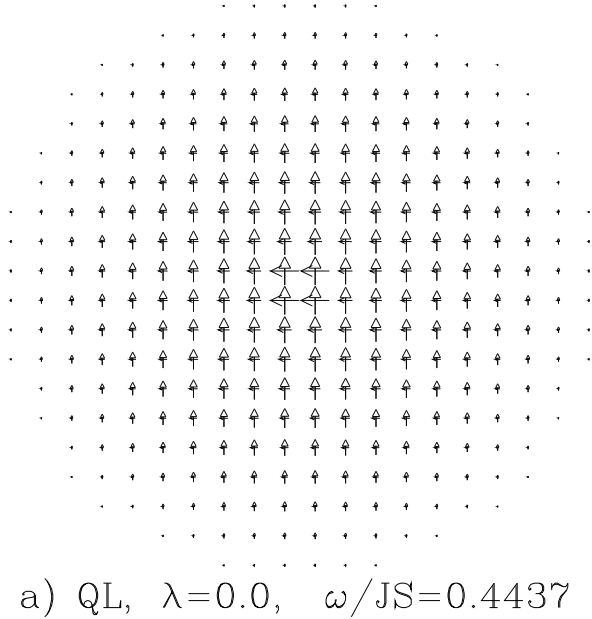b) QL, λ=0.70, ω/JS=0.0486

FIG. 5. The wavefunction for the FM quasi-local mode, in the $R = 10$ system. Open arrows ($\rightarrow$) represent the complex coefficients $w_{k,\mathbf{n}}^{(1)}$ (out-of-plane fluctuations) and closed arrows ($\longrightarrow\!\!\!\triangleright$) represent $w_{k,\mathbf{n}}^{(2)}$ (in-plane fluctuations). a) $\lambda = 0.0$, with $w_{k,\mathbf{n}}^{(1)}$ arrows exaggerated by a factor of 4 relative to $w_{k,\mathbf{n}}^{(2)}$ arrows, but phase relations preserved. b) $\lambda = 0.70 \approx \lambda_c$, with $w_{k,\mathbf{n}}^{(2)}$ arrows exaggerated by a factor of 6. c) $\lambda = 0.88$, with $w_{k,\mathbf{n}}^{(1)}$ arrows exaggerated by a factor of 2.

this mode was presented in Ref. [18], for example, the rms size of this wavefunction was found to decrease sharply near λ_c.
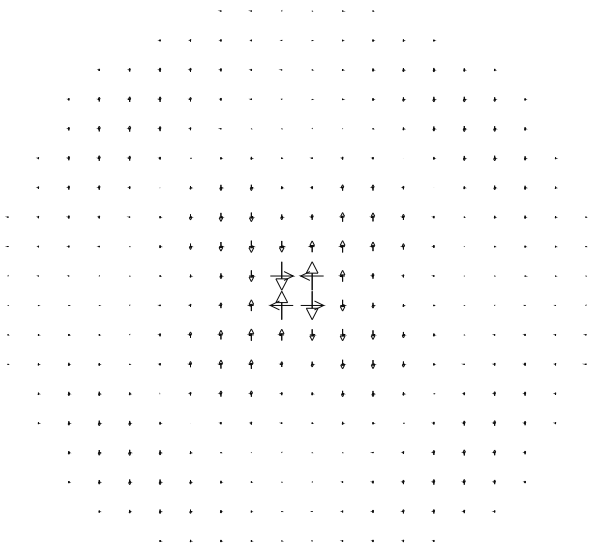
2. AFM: Local Mode Wavefunction

The AFM local mode (LM) wavefunction is shown for several different anisotropies in Fig. 6 for the $R = 10$ system. Again we use the same notation as for the FM wavefunctions and present the complex amplitudes $w_{k,\mathbf{n}}^{(1)}$ and $w_{k,\mathbf{n}}^{(2)}$ as arrows. The in-plane spin fluctuations are quite weak and difficult to see in this mode which is dominated by out-of-plane fluctuations. The $w_{k,\mathbf{n}}^{(1)}$ arrows are seen to be out-of-phase on the two different sublattices. In a sense, they have an "optical motion" as opposed to the "acoustic motion" (two sublattices are in-phase) of the spins in the quasi-local mode of the FM vortex. By using Eq. (4.9b), it is seen that the optical motion of the local mode translates into large continuum out-of-plane fluctuation, ϑ_ℓ. On the other hand, out-of-phase motion of the $w_{k,\mathbf{n}}^{(2)}$ arrows is also present for the local mode, and


c) QL, λ=0.88, ω/JS=0.1539
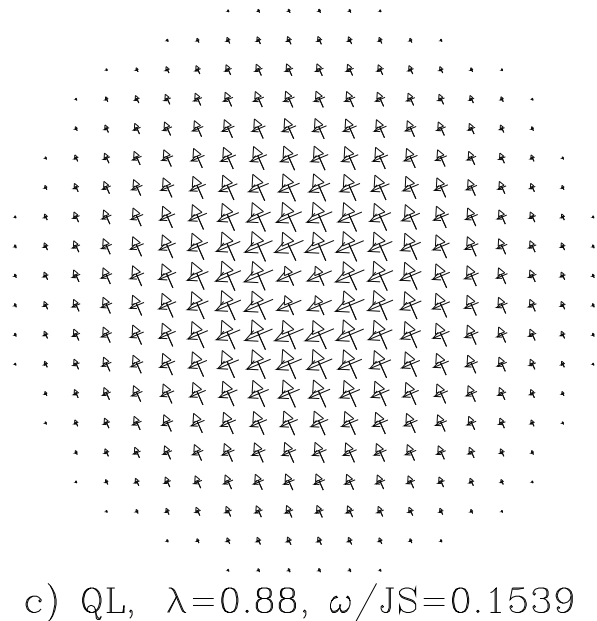
by Eq. (4.9a), this optical motion translates into very small continuum in-plane fluctuation, φ_ℓ. Both of the variables φ_ℓ and ϑ_ℓ follow the form of Eq. (6.1) with winding number $m = 0$, i.e., all sites on one sublattice move completely in phase.

This mode is truly local, in the sense that when the diagonalization is done on larger and larger systems, its

a) LM, λ=0.0, ω/JS=1.4196
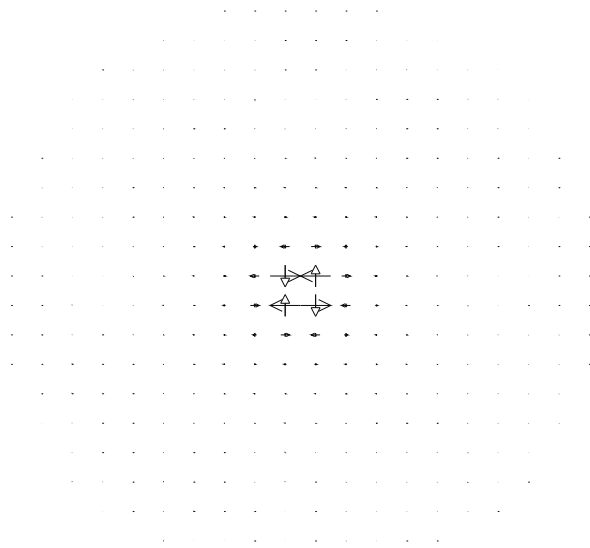
b) LM, λ=0.70, ω/JS=0.1434

FIG. 6. The wavefunction for the AFM local mode, in the $R = 10$ system, with notation as in Fig. 5. a) $\lambda = 0.0$, with $w_{k,\mathbf{n}}^{(1)}$ and $w_{k,\mathbf{n}}^{(2)}$ arrows in the same scale. b) $\lambda = 0.70 \approx \lambda_c$, with $w_{k,\mathbf{n}}^{(2)}$ arrows exaggerated by a factor of 8. c) $\lambda = 0.88$, with $w_{k,\mathbf{n}}^{(1)}$ and $w_{k,\mathbf{n}}^{(2)}$ arrows in the same scale.

frequency converges to a value that depends only on the anisotropy parameter λ, and its rms size is primarily determined by λ. The size dependence of frequency and rms size of several modes, including the local mode, are shown in Figs. 7 and 8, for the particular value $\lambda = 0.88$, which is the point where the LM frequency is maximum, with a value near $1.61JS/\hbar$. The frequencies of other modes, such as the translation mode, decrease with increasing system radius R. The rms sizes of other modes increase strongly with R. The LM rms size possibly shows a weak increase with system size, however, at certain system sizes ($R = 13, 19$) its strong mixing with a nearby "continuum" mode leads to an anomalously large rms size. With this exception, the local mode is truly a mode of the vortex itself, and provided the system used is large enough, is only weakly affected by the boundaries.

C. The Translational Modes

For the translation modes (marked in the Figures by T where degenerate, or TL and TH where nondegenerate), the result is simplest for the AFM. There the translational mode is doubly degenerate for any λ, and correspondingly, for either the in-plane or out-of-plane vortex. However, the translation mode frequency has a distinct

c) LM, λ=0.88, ω/JS=1.6181
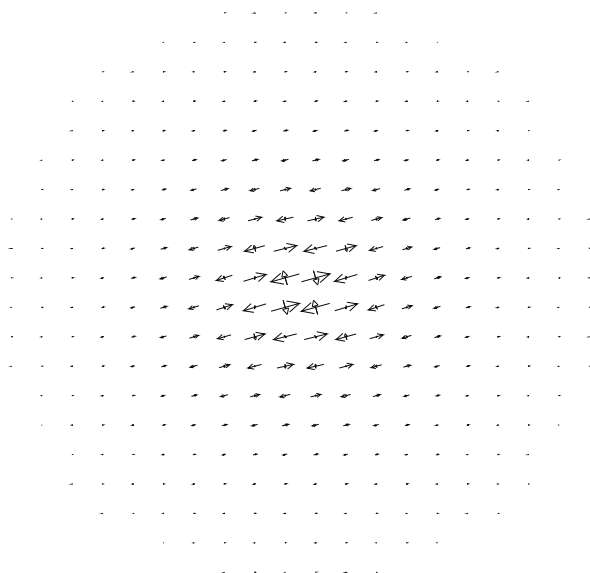
cusp at λ_c, and then falls towards much lower frequency for $\lambda > \lambda_c$. Its frequency is not zero, as would be usual for a translational mode, due to the pinning potentials of the discrete lattice. The double degeneracy is in some vague sense related to the two different directions of motion possible for the vortex, however, it is more deeply connected to the symmetry of the AFM vortices with re-
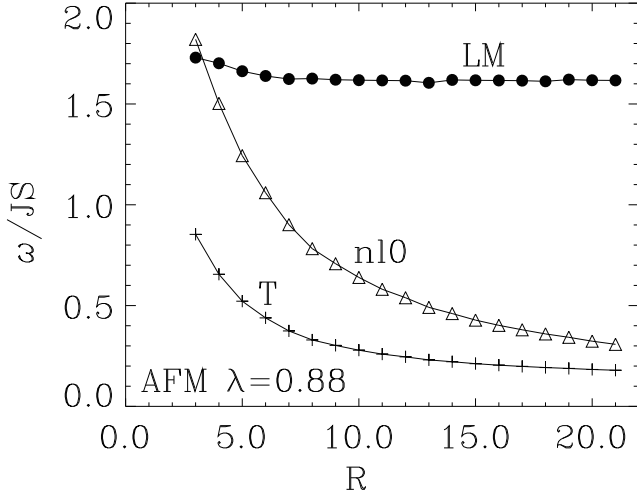
FIG. 7. The AFM local mode (LM), translation mode (T) and $m = 0$ nonlocal mode (nl0) frequencies vs. system radius R, for $\lambda = 0.88$. (see Figs. 6,11, and 12).
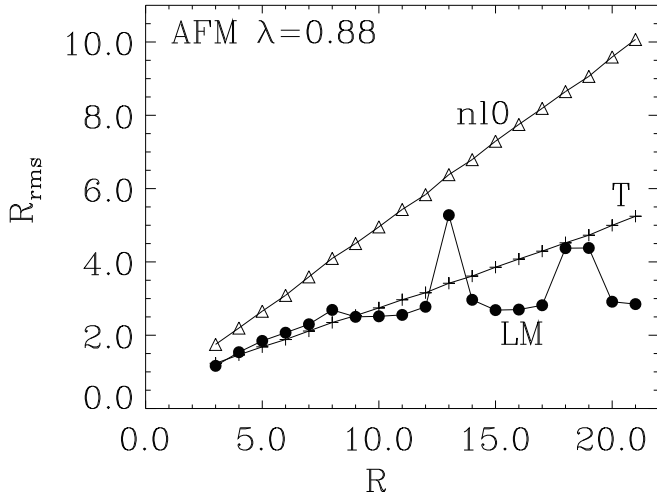

FIG. 8. The AFM local mode (LM), translation mode (T) and $m = 0$ nonlocal mode (nl0) *rms* sizes R_{rms} vs. system radius R, for $\lambda = 0.88$. (see Figs. 6,11, and 12).

spect to reversing S^z and interchanging sublattices. In the FM, however, this operation reverses the sign of the polarization and therefore the gyrovector, whose coupling to the winding number induces the splitting according to expression (6.2).

For the FM vortices, the translation modes are more interesting. For the in-plane vortex ($\lambda < \lambda_c$), the translation modes are doubly degenerate, as in the AFM. For the out-of-plane vortex ($\lambda > \lambda_c$), however, this degeneracy is split, and there is a considerable difference in frequency of the two translation modes, marked by TL and TH. To understand the reason for this splitting, it is

necessary to consider the wavefunctions associated with the modes, and also to verify what motions result when a small amplitude of any of these modes is added to the original static vortex structure. We see immediately below that the translational modes have winding numbers $m = \pm 1$, and this fact is the source of the splitting for the FM but not for the AFM model.
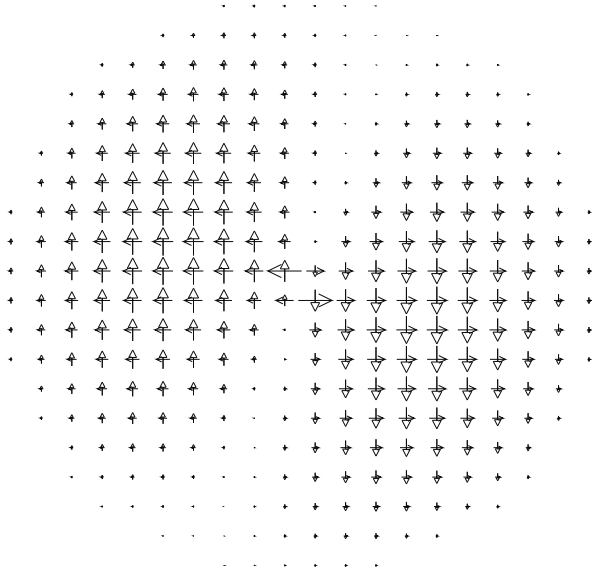
1. FM Translational Modes: Wavefunctions and Motions

Typical arrow diagrams for the FM translational modes of a $R = 10$ system are shown in Figures 10 (TL) and 9 (TH), for both the in-plane ($\lambda = 0$) and out-of-plane ($\lambda = 0.88$) vortices. By adding a small amplitude of any mode to the static vortex structure, and then evolving it according to its known $e^{i\omega t}$ time dependence, one can observe the particular spin motions associated with the mode, as well as the motion of the vortex center it causes. Consider $\lambda = 0$. The mode in part a) of Fig. 10 produces linear vortex motion approximately in the "x" direction, while the other translation mode in part a) of Fig. 9 produces linear vortex motion in the "y" direction. Furthermore, by considering the spin arrows, for $\lambda = 0$ these modes are mixtures of $m = +1$ amd $m = -1$ states. The relative phases in the mixture result in the different orientations of the modes and the different directions of motion. But since $m = +1$ and $m = -1$ are degenerate, we could just as well have shown the wavefunctions for the "pure" states, which would have resulted in two modes each corresponding to circular motions in the two opposite senses.

For $\lambda = 0.88$, the spin arrows in part b) of Fig. 10 are now seen to behave with only the $m = -1$ winding number. The motion that results from this mode is circular motion in the clockwise sense. Now it is not degenerate with the other (higher) translation mode in Fig. 9b, which is seen to have $m = +1$ and causes circular motion in the counterclockwise sense. The static vortex used had polarization $p = +1$, vorticity $q = +1$, and therefore positive gyrovector $G = +2\pi$. Thus it appears that translation mode that makes the product Gm negative has the lower frequency, and produces vortex circular motion in the sense opposite to that determined by using the right hand rule applied to the gyrovector.

2. AFM Translational Modes: Wavefunctions and Motions

Typical arrow diagrams for the AFM translational modes of a $R = 10$ system are shown in Figure 11 (T), for both the in-plane ($\lambda = 0$) and out-of-plane ($\lambda = 0.88$) vortices. In this case, we show only one mode, as the other mode is similar but just rotated by 90°. The mode shown produces linear motion in the x-direction even for $\lambda > \lambda_c$. That is, the two translation modes remain degenerate for all λ, and there is no energy difference for

10
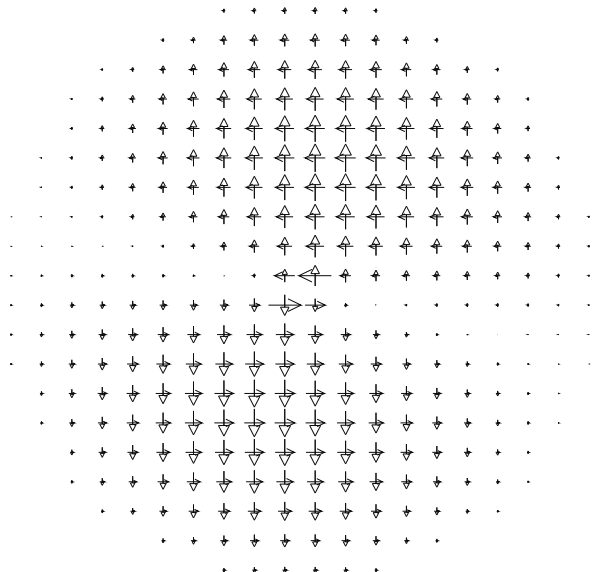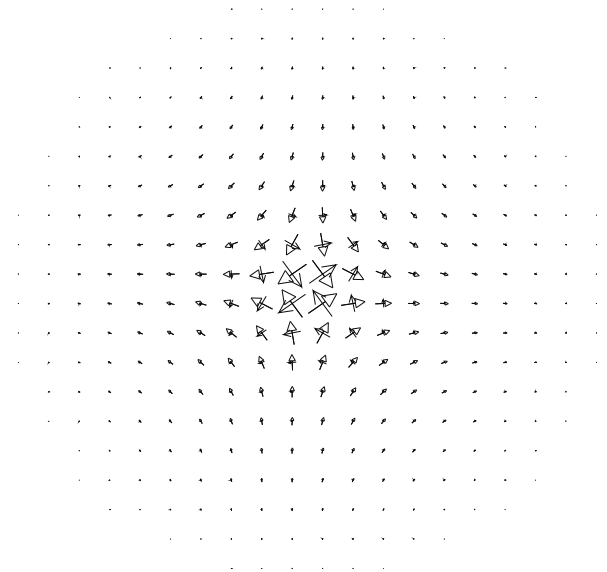
a) T, $\lambda=0.0$, $\omega/JS=0.6926$
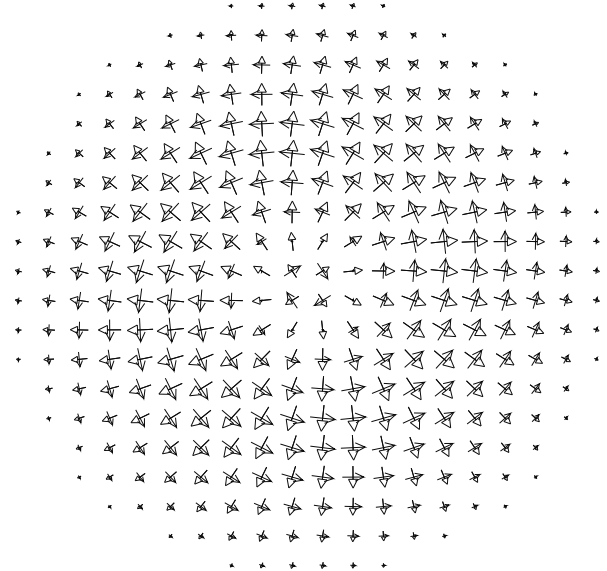
b) TH, $\lambda=0.88$, $\omega/JS=0.2682$

FIG. 9. (above) Wavefunction for the higher translational mode (TH) of the FM model, using arrows as explained in Fig. 5. a) $\lambda = 0.0$, with $w_{k,\mathbf{n}}^{(1)}$ arrows exaggerated by a factor of 4. b) $\lambda = 0.88$, with $w_{k,\mathbf{n}}^{(1)}$ arrows exaggerated by a factor of 2. In b), this mode has winding number $m = +1$ and produces a counterclockwise motion of the vortex center.

FIG. 10. (below) Wavefunction for the lower translational mode (TL) of the FM model, using arrows as in Fig. 5. a) $\lambda = 0.0$, with $w_{k,\mathbf{n}}^{(1)}$ arrows exaggerated by a factor of 4. b) $\lambda = 0.88$, with $w_{k,\mathbf{n}}^{(1)}$ and $w_{k,\mathbf{n}}^{(2)}$ arrows in the same scale. In b), this mode has winding number $m = -1$ and produces a clockwise motion of the vortex center.

a) T, $\lambda=0.0$, $\omega/JS=0.6926$

b) TL, $\lambda=0.88$, $\omega/JS=0.0152$

a) T, $\lambda = 0.0$, $\omega/JS = 0.6930$
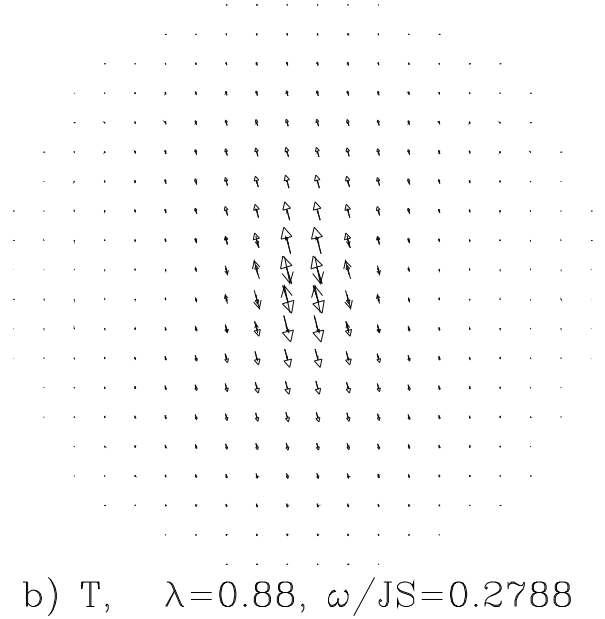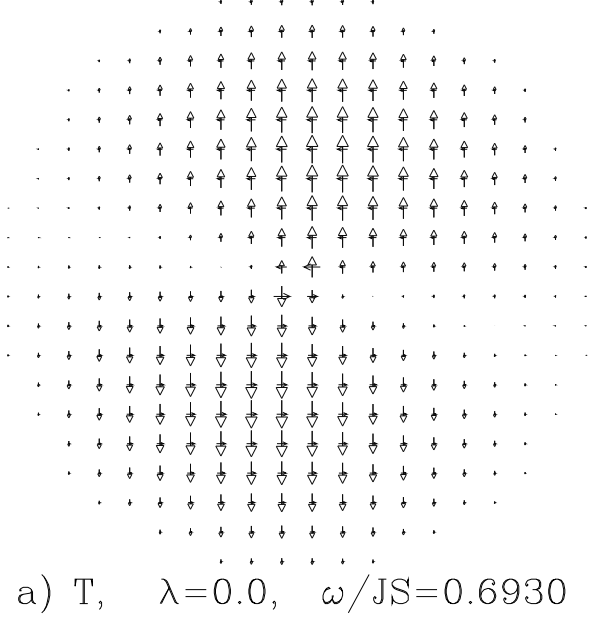

b) T, $\lambda = 0.88$, $\omega/JS = 0.2788$

FIG. 11. Wavefunction for one of the translational modes (T) of the AFM model, using arrows as described in Fig. 5. a) $\lambda = 0$, with $w_{k,\mathbf{n}}^{(1)}$ arrows exaggerated by a factor of 2. b) $\lambda = 0.88$, with $w_{k,\mathbf{n}}^{(1)}$ and $w_{k,\mathbf{n}}^{(2)}$ arrows in the same scale. This mode is a mixture of $m = \pm 1$ states and produces a linear motion of the vortex center approximately in the x-direction.

circular motion in the clockwise sense compared to the counterclockwise sense. The basic translation modes can be taken as linear combinations of $m = +1$ and $m = -1$ states to produce linear motions. Again, there is no splitting of the $m = \pm 1$ states because the gyrovector for AFM vortices is identically zero, due to a cancellation of contributions from the different sublattices.

D. AFM: Nonlocal $m = 0$ Mode

For comparison with the local mode wavefunction, we also show the other low frequency $m = 0$ mode wavefunction in Fig. 12. This mode is the lowest frequency mode at $\lambda = 0$ (See Figs. 2b, 3b and 4b) and undergoes no particular changes as a function of λ. The mode is spread out over the system, and is dominated by the $w^{(1)}$ (in-plane) fluctuations–in the Figure the out-of-plane fluctuations have been exaggerated by a factor of 4 so they can be seen. The other important difference compared to the local mode shown in Fig. 6 is that the $w^{(1,2)}$ arrows on the two sublattices are in phase with each other for this mode, as opposed to the out-of-phase behavior in the local mode. This is effectively an acoustic motion, in contrast to the optical motion in the local mode. By

using Eq. (4.9b), the acoustic motion of $w_{k,\mathbf{n}}^{(1)}$ translates into small continuum out-of-plane fluctuation ϑ_ℓ, and by Eq. (4.9a), the acoustic motion of $w_{k,\mathbf{n}}^{(2)}$ translates into large continuum in-plane fluctuation φ_ℓ.
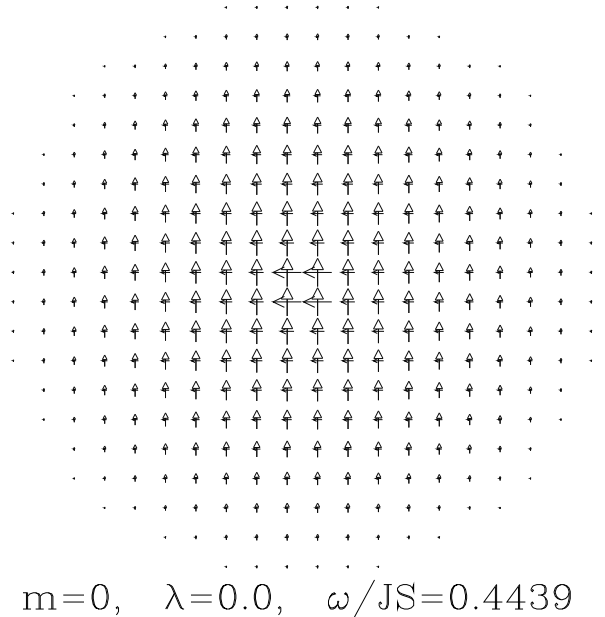

m=0, $\lambda = 0.0$, $\omega/JS = 0.4439$

FIG. 12. Wavefunction for the acoustic $m = 0$ mode (nl0) of the AFM model, for $\lambda = 0$, using the notation of Fig. 5. The $w_{k,\mathbf{n}}^{(1)}$ arrows have been exaggerated by a factor of 4.

12

VII. CONCLUSIONS

We have compared the (low-lying) spin wave modes of easy-plane FM and AFM models in the presence of a single static vortex for different values of the anisotropy parameter λ.

Spectra—For $\lambda < \lambda_c$ we find both models have similar spectra with single and degenerate modes, the latter ones reflecting the mirror symmetry with respect to the easy-plane (which is not destroyed by the presence of a single static in-plane vortex). For $\lambda > \lambda_c$ the spectra for FM and AFM show distinct differences. In the AFM a nonzero out-of-plane component does not destroy the mirror symmetry of the system, because the spins of the two sublattices point in opposite z-directions, and the degenerate modes remain. The nonzero out-of-plane component for an FM vortex, on the other hand, destroys the mirror symmetry, generates a nonzero gyrovector, and according to Eq. (6.2), all degenerate modes split at λ_c.

The soft mode—The crossover from the in-plane vortex for $\lambda < \lambda_c$ to the out-of-plane vortex above λ_c is accompanied by a particular mode which becomes soft at λ_c. In the FM system this mode is quasi-local, i.e. its frequency decreases and its rms size increases as the system size increases, even though it becomes localized around the vortex center close to λ_c. In the FM with the Dirichlet boundary condition used, this mode is always the lowest lying one for $\lambda < \lambda_c$.

For the AFM system, in contrast, this soft mode is a truly localized mode, and its frequency is independent of the system size. This leads to "mode crossing" for increasing system size, when the non-local modes decrease in frequency and the local mode falls well within continuum modes. The mixing with other modes leads to sudden increases in the rms size of the local mode, but away from these situations, the LM rms size has only a weak dependence on the system size, and is considerably less than the rms size of other modes of similar frequency. The LM frequency peaks at the value $\omega/JS \approx 1.61$ for $\lambda \approx 0.88$, while the rms size is around 3 lattice constants except when the mixing occurs.

In both systems there are non-local modes higher up the spectra, which also show distinct downward cusps at λ_c. These modes show a similar symmetry as the (quasi-) local mode.

The translation modes—The first degenerate mode for $\lambda < \lambda_c$ in both models corresponds to translational motion of the vortex. The degeneracy shows that the vortex motion is equivalent in both independent directions for λ_c (x- and y-translation or left- and right-rotation). For the AFM this is also true above λ_c, though the softening of the two translational modes indicate that the out-of-plane vortex moves "easier" than the in-plane vortex (due to the extended out-of-plane structure which helps to overcome discreteness effects). The translational mode in the FM system splits at λ_c with one mode (TL) softening (as in the AFM model), the other (TH) hardening

slightly from its frequency at λ_c. This indicates that the translational motion of the vortex in one of the two independent directions is favored. The inequivalency of the two directions is a direct consequence of the coupling of the winding number $m = \pm 1$ for the translation modes with the nonzero gyrovector, as mentioned in Eq. (6.2). For an out-of-plane vortex with positive vorticity ($q = +1$) and positive polarization ($p = +1$), the lower translation mode has winding number $m = -1$ while the higher translation mode has $m = +1$. This is the result for a positive gyrovector $G = 2\pi pq$; the winding numbers of the lower and higher translation modes will be interchanged for a vortex with negative gyrovector. We should also mention that the net motion that results in these modes is partly determined by the Dirichlet type boundary condition we have applied, which exerts an effective force on the vortex towards the center of the system. Thus, the results presented here will be important for further analysis of vortex dynamical equations of motion which consider combined effects due to gyrovector, external forces, and vortex effective mass [13,22].

[1] See, for example, L.P. Regnault and J. Rossat-Mignod, J. Magn. Magn. Mater. **14**, 194 (1974); L.P. Regnault et al., Physica B+C, **136B**, 329 (1986); L.M. Falicov and J.L. Moran-Lopez, editors., "Magnetic Properties of Low-Dimensional Systems," Springer-Verlag, Berlin (1986).

[2] V.L. Berezinskii, Sov. Phys. JETP **34**, 610 (1972).

[3] J.M. Kosterlitz and D.J. Thouless, J. Phys. C **6**, 1181 (1973); *ibid.*, C **7**, 1046 (1974).

[4] S. Hikami and T. Tsuneto, Prog. Theor. Phys. **63**, 387 (1980).

[5] S. Takeno and S. Homma, Prog. Theor. Phys. **65**, 172 (1980).

[6] M.E. Gouvêa, G.M. Wysin, A.R. Bishop and F.G. Mertens, Phys. Rev. B**39**, 11840 (1989).

[7] F.G. Mertens, A.R. Bishop, G.M. Wysin and C. Kawabata, Phys. Rev. Lett. **59**, 117 (1987); Phys. Rev. B **39**, 591 (1989).

[8] B.V. Costa, M.E. Gouvêa and A.S.T. Pires, Phys. Lett. A **165**, 179 (1992).

[9] A.R. Pereira, A.S.T. Pires and M.E. Gouvêa, Solid St. Comm. **86**, 187 (1993).

[10] A.R. Pereira, A.S.T. Pires and M.E. Gouvêa, J. Magn. Magn. Mater. **134**, 121 (1994).

[11] A.A. Thiele, Phys. Rev. Lett. **30**, 230 (1973); J. Appl. Phys. **45**, 377 (1974).

[12] D.L. Huber, Phys. Lett. 76A, 406 (1980); Phys. Rev. B 26,, 3758 (1982).

[13] G.M. Wysin and F.G. Mertens, in *Nonlinear Coher-*

ent Structures in Physics and Biology, Lecture Notes in Physics **393**, Springer-Verlag, Berlin (1991); G.M. Wysin, F.G. Mertens, A.R. Völkel and A.R. Bishop, in *Nonlinear Coherent Structures in Physics and Biology*, Plenum, New York (1994).

[14] A.R. Völkel, G.M. Wysin, F.G. Mertens, A.R. Bishop and H.J. Schnitzer, Phys. Rev. B **50**, 12,711, (1994).

[15] B. A. Ivanov and A. K. Kolezhuk, Phys. Rev. Lett. **74**, 1859 (1995).

[16] A.R. Völkel, F.G. Mertens, A.R. Bishop and G.M. Wysin, Phys. Rev. B**43**, 5992 (1991).

[17] G.M. Wysin, Phys. Rev. B **49**, 8780 (1994).

[18] G. M. Wysin and A. R. Völkel, Phys. Rev. B **52**, 7412 (1995).

[19] G.M. Wysin, M.E. Gouvêa, A.R. Bishop and F.G. Mertens, in "Computer Simulations Studies in Condensed Matter Physics," D.P. Landau et al., eds., Springer-Verlag, Berlin (1988).

[20] B. A. Ivanov, A. K. Kolezhuk and G. M. Wysin, Phys. Rev. Lett. **76**, 511 (1996).

[21] R. Boesch, P. Stanicoff and C.R. Willis, Phys. Rev. B **38**, 6713 (1988); R. Boesch and C.R. Willis, Phys. Rev. B **42**, 6371 (1990).

[22] F.G. Mertens, G. Wysin, A.R. Völkel, A.R. Bishop and H.J. Schnitzer, in "Nonlinear Coherent Structures in Physics and Biology," F.G. Mertens and K.H. Spatschek, eds., Plenum, New York (1994).

[23] A similar gradient term for the 1D AFM is present in Eq. (3) for $\vec{m}$ of Ref. [15], whose static limit, however, does not give $\vec{m} = 0$. For $\lambda \approx 1$, an alternative expression of Eq. 4.4 is [20] $\vec{m} = (\hbar/8JS)\vec{\ell} \times \dot{\vec{\ell}}$, and which is valid for both the static and dynamic spin fields in the absence of an external magnetic field.

[24] B. A. Ivanov, private communication.

[25] A. R. Völkel, F. G. Mertens, G. M. Wysin and A. R. Bishop, J. Magn. Magn. Mater. **104-107**, 766 (1992).